MIT Open Access Articles

SUZAKU OBSERVATIONS OF 4U 1957+11: POTENTIALLY THE MOST RAPIDLY SPINNING BLACK HOLE IN (THE HALO OF) THE GALAXY

SUZAKU OBSERVATIONS OF 4U 1957+11: POTENTIALLY THE MOST RAPIDLY SPINNING BLACK HOLE IN (THE HALO OF) THE GALAXY

Michael A. Nowak[1], Jörn Wilms[2], Katja Pottschmidt[3], Norbert Schulz[1], Dipankar Maitra[4], and Jon Miller[4]

[1] Massachusetts Institute of Technology, Kavli Institute for Astrophysics, Cambridge, MA 02139, USA; mnowak@space.mit.edu, nss@space.mit.edu
[2] Dr. Karl Remeis-Sternwarte and Erlangen Centre for Astroparticle Physics, Universität Erlangen-Nürnberg,
Sternwartstr. 7, 96049 Bamberg, Germany; joern.wilms@sternwarte.uni-erlangen.de
[3] CRESST, UMBC, and NASA Goddard Space Flight Center, Greenbelt, MD 20771, USA; katja@milkyway.gsfc.nasa.gov
[4] Department of Astronomy, University of Michigan, 500 Church Street, Ann Arbor, MI 48109-1042, USA; dmaitra@umich.edu, jonmm@umich.edu

ABSTRACT

We present three *Suzaku* observations of the black hole candidate 4U 1957+11 (V1408 Aql)—a source that exhibits some of the simplest and cleanest examples of soft, disk-dominated spectra. 4U 1957+11 also presents among the highest peak temperatures found from disk-dominated spectra. Such temperatures may be associated with rapid black hole spin. The 4U 1957+11 spectra also require a very low normalization, which can be explained by a combination of small inner disk radius and a large distance (>10 kpc) which places 4U 1957+11 well into the Galactic halo. We perform joint fits to the *Suzaku* spectra with both relativistic and Comptonized disk models. Assuming a low-mass black hole and the nearest distance ($3\,M_\odot$, 10 kpc), the dimensionless spin parameter $a^* \equiv Jc/GM^2 \gtrsim 0.9$. Higher masses and farther distances yield $a^* \approx 1$. Similar conclusions are reached with Comptonization models; they imply a combination of small inner disk radii (or, equivalently, rapid spin) and large distance. Low spin cannot be recovered unless 4U 1957+11 is a low-mass black hole that is at the unusually large distance of $\gtrsim 40$ kpc. We speculate whether the suggested maximal spin is related to how the system came to reside in the halo.

Key words: accretion, accretion disks – black hole physics – radiation mechanisms: thermal – X-rays: binaries

Online-only material: color figures

1. INTRODUCTION

4U 1957+11 is one of the few black hole candidates (BHC), such as LMC X-1, LMC X-3, and Cyg X-1, that historically has been persistently active. In contrast to these other sources, however, it is a low-mass X-ray binary (LMXB; see Thorstensen 1987; Hakala et al. 1999; Russell et al. 2010; Bayless et al. 2011). Also in contrast to other persistent Galactic BHC sources, 4U 1957+11 apparently has remained always in a spectrally soft state (Nowak et al. 2008). Its soft spectrum is well modeled as a simple disk (Nowak & Wilms 1999; Wijnands et al. 2002; Nowak et al. 2008; Dunn et al. 2010), i.e., a multi-temperature blackbody (Mitsuda et al. 1984) characterized by a peak temperature and a normalization related to the disk inner radius, inclination, and object distance. Approximately 15% of the over 40 pointed observations taken with the *Rossi X-ray Timing Explorer* (*RXTE*), however, also show a significant contribution (20%–75% of the observed 3–18 keV flux) from a non-thermal/steep power-law component (Nowak et al. 2008; Dunn et al. 2010).

Optical observations suggest that we may be viewing the disk in 4U 1957+11 at a high inclination of ∼75°. Modulation over a 9.33 hr orbital period has ranged from ±10% and sinusoidal (Thorstensen 1987) to ±30% and complex (Hakala et al. 1999). The latter has been interpreted as a high-inclination warped disk being partly occulted by the secondary. On the other hand, Russell et al. (2010) failed to find any optical modulation over the orbital period, while Bayless et al. (2011) found nearly sinusoidal modulation. These latter authors attributed the optical modulation to illumination of the secondary, and noting a lack of any flattening at the light-curve minimum, they modeled the

system inclination with values as low as 20° and not greater than 70°.

Currently, the mass, distance, and inclination of 4U 1957+11 are unknown. Based upon a comparison of the optical flux to the estimated optical luminosities of other BHC, however, Russell et al. (2010) have argued that 4U 1957+11 must lie at a distance >20 kpc. The possibility of a high inclination, however, makes such comparisons problematic. Russell et al. (2011) recently have presented near-simultaneous radio (*Expanded Very Large Array*, *EVLA*), optical (*Faulkes Telescope North*), and UV/X-ray (*Swift*) observations of 4U 1957+11. These observations show the soft-state flux to be extremely quenched (factors of 330–810 times lower than the expected radio/X-ray flux ratio for hard-state black hole sources) and demonstrate that the optical/UV flux is roughly consistent with the expectation of an irradiated disk. Those observations, however, do not definitively constrain the source's inclination or distance. A minimum distance of >5 kpc; however, has been determined via high-resolution X-ray spectroscopy. Ne IX 13.45 Å absorption, associated with the warm/hot phase of the interstellar medium (ISM), is detected with a sufficient equivalent width to suggest that 4U 1957+11 resides above the galactic plane at this minimum distance or beyond (Yao et al. 2008; Nowak et al. 2008).

Nowak et al. (2008) showed that, with the exception of the ≈15% of the time when a non-thermal component becomes prominent, disk models of the soft X-ray component have an approximately constant radius but a temperature that increases with flux (see Figure 9 of Nowak et al. 2008). There is some indication for a slight increase in disk radius at the lowest flux levels, which was interpreted as possibly being associated with the source approaching a transition to a spectrally hard

state. Such a transition is expected to occur at 2%–3% L_{Edd}, where L_{Edd} is the Eddington luminosity for the source in question (Maccarone 2003). At the other extremes of flux in 4U 1957+11, the simple disk spectrum "drops out" (disk radius decreases in disk+power-law fits, or disk temperature decreases in disk+Compton corona fits) and is replaced by the non-thermal/steep power-law component (Nowak et al. 2008).

Although other persistent systems transiently show disk-dominated spectra,[5] the persistent, soft spectra of 4U 1957+11 are perhaps the simplest and cleanest examples of "disk spectra." *XMM-Newton* and *Chandra* observations show that there is very little absorption ($N_H = 1$–2×10^{21}cm^{-2}), while *RXTE* observations show that a hard tail contributes usually <20% of the flux. Furthermore, any additional components such as a broad Fe line (typically <2% peak residual in the fits) or a "smeared Fe edge" (which was never required or indicated in any of the *RXTE* spectra; Nowak et al. 2008) are very weak or absent. Thus, the soft spectrum of 4U 1957+11 becomes the ideal testbed for modern disk atmosphere models that incorporate spin and other general relativistic effects into their calculations (e.g., Li et al. 2005; Davis et al. 2005, 2006; Shafee et al. 2006).

Nowak et al. (2008) showed that the disk fits to the *XMM-Newton*, *Chandra*, and *RXTE* spectra of 4U 1957+11 are characterized by a very low normalization, indicating some combination of large distance and low compact object mass, and very high inner disk temperature (1.3–1.8 keV). In other sources the latter has been associated with high black hole spin. To assess this possibility, Nowak et al. (2008) applied the relativistic disk model, `kerrbb`, of Li et al. (2005). The model parameters include a compact object mass and distance, disk inclination, accretion rate, spectral hardening factor (the ratio of color temperature to effective temperature), and dimensionless spin of the black hole, $a^* \equiv Jc/GM^2$. For a wide variety of masses and distances, fits to the *XMM-Newton* and *Chandra* spectra preferred maximal spin, $a^* \approx 1$. The *RXTE* spectra, in fact, could not be described with low spin, even when including a coronal or power-law component.

Various theoretical models of a disk atmosphere have suggested a spectral hardening factor of ∼1.7. If this is correct, and utilizing the fact that the lowest flux observations must be $\gtrsim$3% L_{Edd}, then the spectral fits of 4U 1957+11 strongly suggest that it is a maximally spinning, ≈16 $M_\odot$ black hole at a distance of ≈22 kpc (Nowak et al. 2008). In this work we explore that claim with three recent *Suzaku* observations.

In Section 2, we describe the *Suzaku* observations and the details of the data processing. We then present the model fits to the resulting spectra in Section 3. Section 4 describes the scaling relations that we used to translate fits using a low-mass, short-distance black hole to comparably good fits involving a larger mass, further distance black hole. We then present our conclusions in Section 5.

2. OBSERVATIONS AND DATA ANALYSIS

The *Suzaku* data were reduced with tools from the HEASOFT v6.9 package and the calibration files current as of 2010 September. The instruments on *Suzaku* (Mitsuda et al. 2007) are the X-ray Imaging Spectrometer (XIS; Koyama et al. 2007) CCD detector covering the ≈0.3–10 keV band, and the Hard X-ray Detector (HXD; Takahashi et al. 2007) comprised of

Table 1
Log of 4U 1957+11 Observations

Date (yyyy-mm-dd)	(MJD)	ObsID	Exposure (ks)
2010-05-04	55320.82	405057010	35.80
2010-05-17	55333.80	405057020	37.20
2010-11-01	55502.19	405057030	15.50

Notes. Exposure times are after good time filtering and represent the maximum exposure in an XIS detector when combining all data modes. MJD is the (non-barycenter corrected) average modified Julian date of the observation.

the PIN diode detector (PIN) covering the ≈10–70 keV band and the gadolinium silicate crystal detector (GSO) covering the ≈60–600 keV band. The XIS had four separate detectors, XIS 0–3, with XIS 1 being a backside illuminated CCD. XIS 2 was lost due to a micrometeor hit in late 2006, and thus we only consider data from the remaining three XIS detectors. For all three observations described here, the hard X-ray fluxes were too low to lead to a significant detection in either of the HXD detectors, and therefore we do not include these data. A log of the observations is found in Table 1.

All of the XIS observations were run in a sub-array mode wherein 1/4 of the CCD was exposed with 2 s integration times. In preparing the XIS spectra, we first corrected each detector for charge transfer inefficiency using the `xispi` tool, and then reprocessed the data with `xselect` using the standard `xisrepro` selection criteria. Due to thermal flexing of the spacecraft, the attitude of the *Suzaku* spacecraft exhibits variability over the course of the observations and therefore the image of the source is not at a fixed position on the CCD. Standard processing reduces this variability and improves the point-spread function (PSF) image (Uchiyama et al. 2008); however, the standard tools do not yet fully correct the variable attitude induced blurring. We created an improved attitude reconstruction, and hence narrower PSF images, using the `aeattcor.sl` software described[6] by Nowak et al. (2011). For the third observation, however, approximately half of the good time intervals (i.e., half of each spacecraft orbit) were affected by wobbles severe enough (>1′) such that a large fraction of the image on the XIS 1 detector fell beyond the boundaries of the detector's active regions. Although the images did not fall beyond the active region boundaries on the XIS 0 and XIS 3 detectors, there are serious questions about the accuracy of the generated response functions for such large off-axis angles. We therefore excluded these times from the spectra and reflect this in Table 1.

Using the image generated from the improved attitude correction, we then used the `pile_estimate.sl` S-Lang script[7] (Nowak et al. 2011) to estimate the degree of pileup in the XIS observations. For the spectra described in this work, the center of the PSF images was affected by as much as a 33% pileup fraction. We therefore exclude two, overlapping rectangular regions (≈15 × 60 pixels, nearly at right angles to one another) aligned along the brightest portions of the central PSF (see Figure 1). We estimate that the remaining residual pileup fractions are $\lesssim$3%.

The outer limit of the extraction area was a rectangular region limited by the 4′ width of the 1/4 array boundaries. Additionally, we extracted background spectra from small rectangular regions, near the edges of the chips, that avoided as much as possible both the 4U 1957+11 image and the

---

[5] LMC X-1 is likely wind-fed, and, for a soft state, shows an unusual and highly variable disk spectrum (Nowak et al. 2001). LMC X-3 cycles through soft/hard-state transitions (Wilms et al. 2001).

[6] See also: http://space.mit.edu/CXC/software/suzaku/aeatt.html.
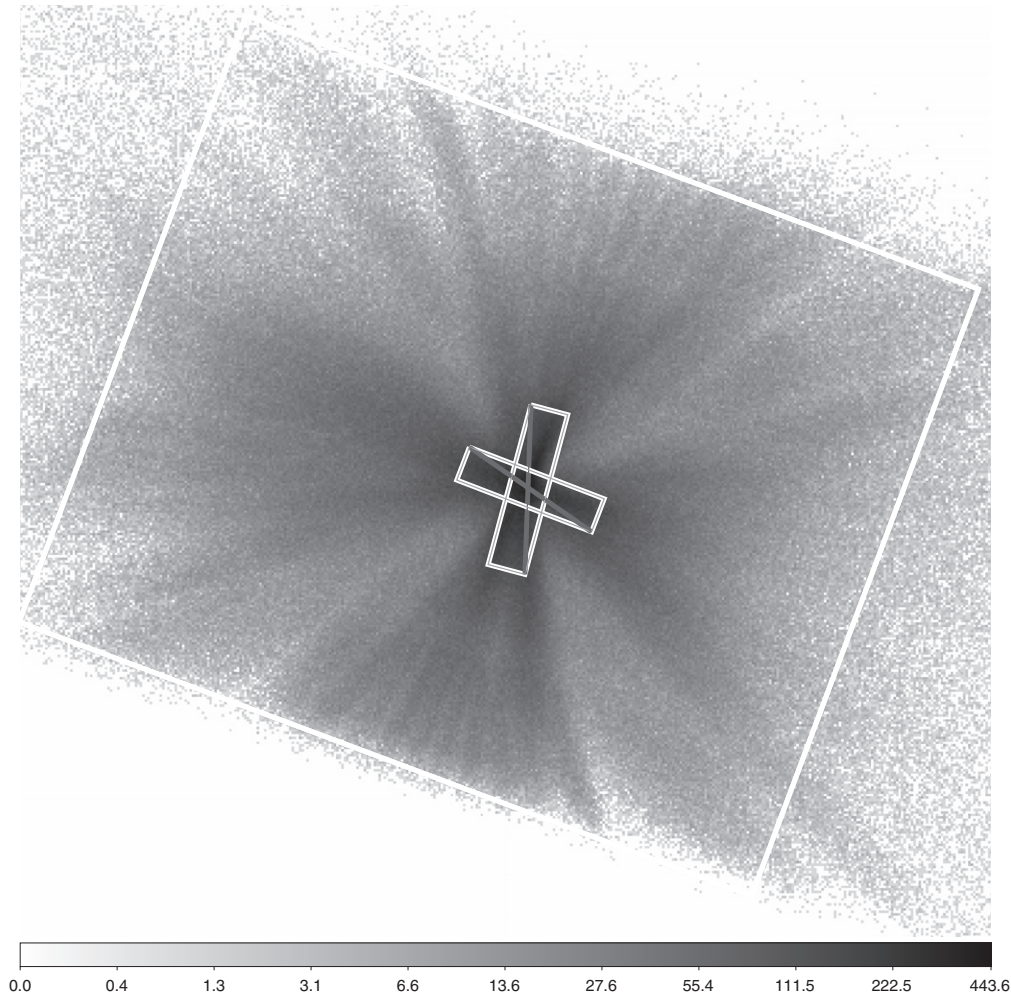[7] http://space.mit.edu/CXC/software/suzaku/pest.html

Figure 1. Aspect corrected XIS 1 0.5–8 kev image on a logarithmic intensity scale from ObsID 405057010. The boxes outline the detector region from which the spectra were generated. The length of the short edge of the outer box is approximately 4.'5. The inner boxed regions with diagonal slashes were excluded from the spectra.

detector images of the on-board calibration sources. It is not entirely clear to what degree these regions are dominated by "true background," as opposed to the wings of the PSF from the source. However, the normalized background flux remains at <2% of the source flux between 0.5 and 8 keV, and thus does not strongly affect the analyses presented in this work. The background flux starts to become an increasingly larger fraction of the source flux above 8 keV. For this reason, as well as due to any other uncertainties in the high-energy calibration of the XIS detectors, we do not consider data above 8 keV.

Events in the XIS detectors were read out from either 3×3 or 5×5 pixel islands. We created individual spectra and response files for each detector and data mode combination. Little source variability was detected over the course of each observation, therefore the spectra were created for the full good time intervals represented by standard processing (excluding the times of very bad attitude errors, discussed above). Response matrices and effective area files were created with the `xisrmfgen` and `xissimarfgen` tools, respectively. For each observation, spectra for the different read-out modes were combined during analysis on a chip-by-chip basis using the `combine_datasets` function within the `Interactive Spectral Interpretation System` (ISIS) fitting program (Houck & Denicola 2000). That is, observations were kept separate, but within an observation all

XIS 0 spectra were combined together, all XIS 1 spectra were combined, etc.

Although spectra for each observation and each XIS chip were kept separate, all spectra were jointly grouped on a common grid such that the XIS 0 spectra for the third (i.e., the faintest and shortest integration time) observation had a minimum combined signal-to-noise ratio (S/N) of 5 in each energy bin ($\approx$25 total counts in each bin, although the estimated background was included in the S/N criterion) and that the minimum number of channels per energy bin was at least the half width half-maximum of the spectral resolution (see Nowak et al. 2011, for a further explanation of this criterion).

In Figure 2, we present the flux-corrected spectra, i.e., the counts spectra divided by the integrated response (see the ISIS user manual for a full description of this process). The spectra show strong deviations from a smooth continuum in the 1.5–2.6 keV region, near X-ray spectral features of Si and Ir. These systematic effects are seen in a wide variety of unrelated *Suzaku* spectra, hence our decision to exclude them from our fits. Likewise, there is a strong spectral feature near 0.55 keV, which we also suspect of being systematic in nature, hence our exclusion of data below 0.7 keV. To avoid these regions of poorly understood response, we only considered spectral energy ranges 0.7–1.5 keV and 2.6–8 keV. The smaller features near 0.75 keV
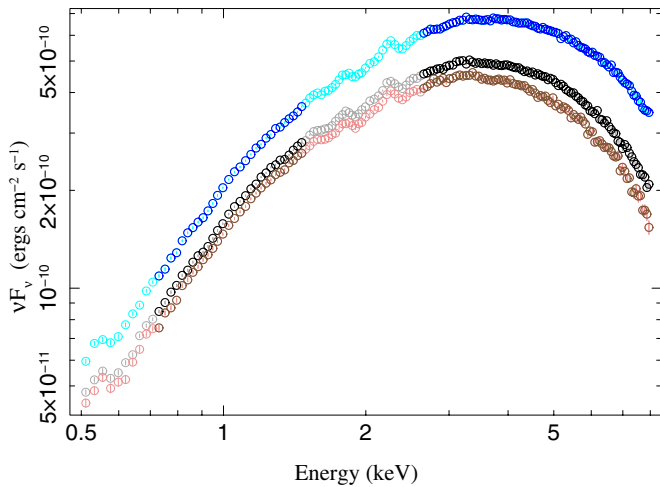
Figure 2. Combined XIS 0, 1, and 3 spectra from each of the three *Suzaku* observations of 4U 1957+11, flux corrected with the detector responses. (ObsID 405057010 is the top spectrum, ObsID 405057020 is the middle spectrum, and ObsID 405057030 is the bottom spectrum.) The three observations share a common binning of approximately half width half-maximum resolution of the detectors. Lighter colored data points represent energy bands that were ignored in the spectral fits described below.

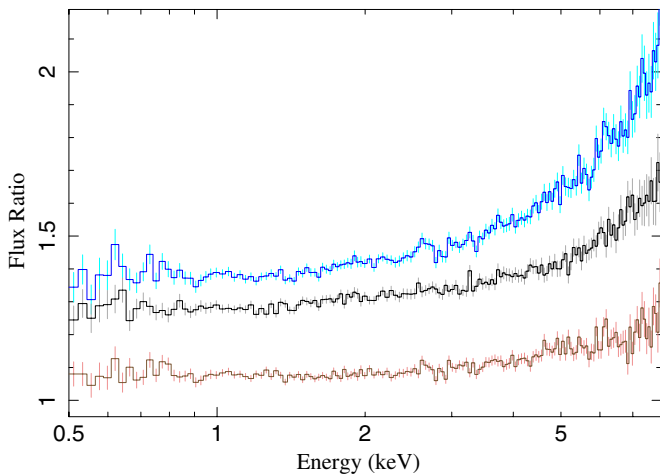(A color version of this figure is available in the online journal.)

Figure 3. Ratios of the flux corrected spectra shown in Figure 2. The top ratio is observation 1/observation 3, the middle line is observation 1/observation2, and the bottom line is observation 2/observation 3.

(A color version of this figure is available in the online journal.)

and 0.9 keV are plausibly associated with Fe L, Ne K, and Ne IX absorption in the ISM, as we discuss below.

The suspected systematic features are relatively constant among the three observations, as is evident from the ratio of the flux corrected spectra as shown in Figure 3. None of the systematic features are seen in these ratios. The ratios are relatively flat $\lesssim 2$ keV, and show a curve upward, with the degree of this curving being greatest for the ratio of the flux corrected spectra for the first and third observations. We discuss this further in the next section.

3. SPECTRAL FITS

The spectral shape shown in Figure 2 , and the ratios seen in Figure 3, are those expected for a disk-dominated spectrum wherein the flux changes are primarily dominated by variations of the peak temperature of the disk. We show the theoretical expectation for such a disk in Figure 4. Here we use the `diskpn`
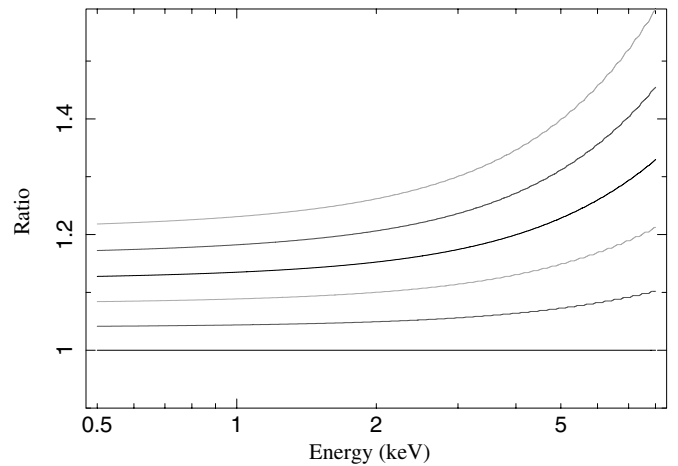

Figure 4. Expectations for the flux ratio in a `diskpn` model when solely changing the peak temperature of the disk. The reference model has a 1.3 keV peak temperature. The peak temperature is varied in steps of 0.05 keV, up to 1.5 keV.

model (Gierliński et al. 1999), which essentially is the spectrum from a Shakura–Sunyaev type disk (Shakura & Sunyaev 1973) calculated using a simple pseudo-Netwonian potential and a no-torque boundary condition at the disk inner edge located at $6\,GM/c^2$. The flux goes to zero at the disk inner edge, and the disk temperature peaks at $\approx 10\,GMc^2$. This basic disk spectrum will underlie the Comptonization fits discussed below.

At energies approximately below the peak temperature, dominated by the Rayleigh–Jeans part of the thermal spectra, the ratios are fairly flat. At energies above the disk peak temperature, on the Wien tail of the thermal spectra, the ratios curve upward. There is a very good correspondence between the curves in Figures 3 and 4. However, based upon our experience with *RXTE* spectra which extended out to ≈ 20 keV, there is the possibility of additional spectral hardening beyond that associated with any rise in disk temperature. We therefore consider the `eqpair` Comptonization model (Coppi 1999) which can use the `diskpn` as its input seed photon spectrum.

Given that the three spectra appear commensurate with a constant disk radius, and that such a nearly constant disk radius is consistent with our experience for $\approx 85\%$ of the *RXTE* spectra that we have previously examined (see Figure 9 of Nowak et al. 2008), we explore a model wherein we fit all three spectra simultaneously with an `eqpair` model for which we constrain the `eqpair` normalization (i.e., the inner disk radius) to be the same for each spectrum. The physical implications of this common normalization are discussed in Section 5.

In addition to constraining the `eqpair` normalization, we also constrain the absorption to be the same for each observation, which we here model with the `TBnew` model (an updated version of the model of Wilms et al. 2000, using the interstellar abundances from that work) and using a fixed Ne IX 13.447 Å absorption line with equivalent width of 7 Å. The latter is consistent with the high spectral resolution studies of Yao et al. (2008) and Nowak et al. (2008, see the below discussion of the ISM absorption). Excluding this component increases the fitted χ^2 by ≈ 12.

For each observation we allow the disk peak temperature, $kT_{\rm disk}$, the coronal compactness, ℓ_h/ℓ_s, and the coronal seed optical depth,[8] τ_s, to be independent parameters. We include

---

8 Table 2, however, presents the *net* optical depth, as `eqpair` includes calculation of the equilibrium pair production in the corona.
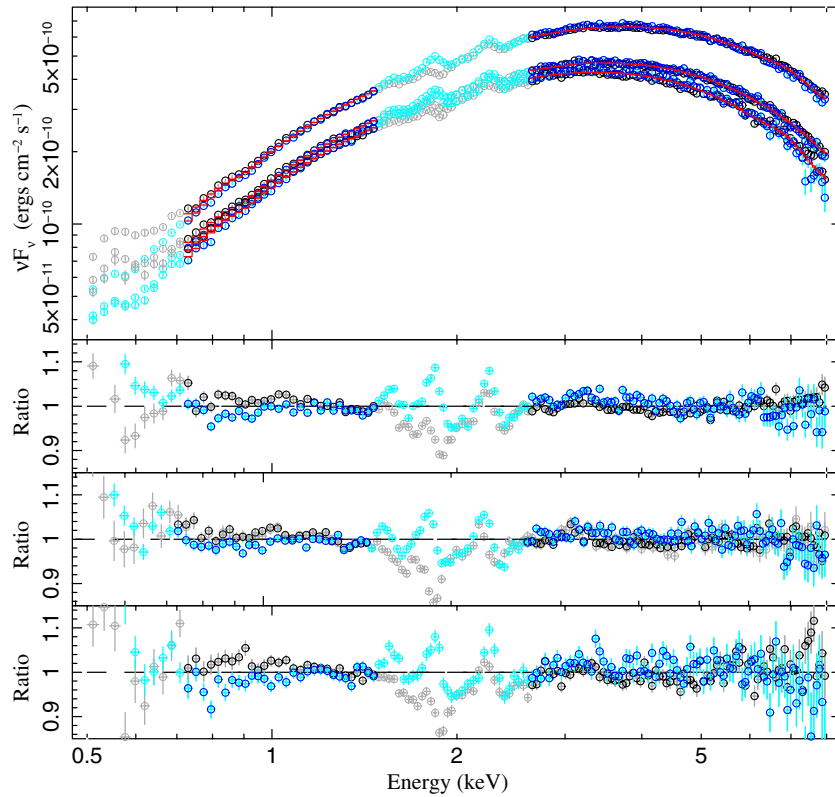
Figure 5. Joint fit of an `eqpair` Comptonization model to the three spectra. The spectra share a common interstellar absorption column and a common normalization (i.e., disk inner radius), but have independent disk temperatures and coronal parameters. Black/gray spectra are the combined XIS 0 and 3 spectra, and blue/light blue are the XIS 1 spectra. Lightly shaded data were not included in the fit. The top residuals' panel shows the ratio residuals for ObsID 405057010, the middle residuals' panel shows the ratio residuals for ObsID 405057020, and the bottom panel shows the ratio residuals for ObsID 405057030.

(A color version of this figure is available in the online journal.)

Table 2
constant*TBnew*(eqpair+gaussian) Fits to 4U 1957+11 Spectra

ObsID	N_H $(10^{21}\,cm^{-2})$	N_{eqp} (10^{-4})	kT_{disk} (keV)	ℓ_h/ℓ_s	τ_{net}	N_γ (10^{-4})	C_{xis0}	C_{xis3}	0.7–8 keV Flux $(10^{-9}\,erg\,cm^{-2}\,s)$	χ^2/dof
405057010	$0.200^{+0.001}_{-0.001}$	$1.926^{+0.001}_{-0.001}$	$1.477^{+0.001}_{-0.001}$	$0.37^{+0.03}_{-0.02}$	$0.017^{+0.002}_{-0.002}$	$1.4^{+0.4}_{-0.5}$	$1.019^{+0.002}_{-0.002}$	$1.020^{+0.002}_{-0.002}$	1.09 ± 0.01	1750.4/1014
405057020	...	...	$1.342^{+0.001}_{-0.001}$	$0.05^{+0.01}_{-0.01}$	$2.4^{+0.1}_{-0.1}$	$0.1^{+0.2}_{-0.1}$	$1.078^{+0.002}_{-0.002}$	$1.083^{+0.002}_{-0.002}$	0.80 ± 0.04	...
405057030	...	...	$1.310^{+0.001}_{-0.001}$	$0.04^{+0.01}_{-0.01}$	$4.4^{+0.1}_{-0.1}$	$1.3^{+0.4}_{-0.4}$	$1.067^{+0.002}_{-0.002}$	$1.057^{+0.003}_{-0.003}$	0.72 ± 0.03	...
405057010	$0.199^{+0.007}_{-0.008}$	$1.926^{+0.002}_{-0.002}$	$1.476^{+0.001}_{-0.001}$	$0.38^{+0.03}_{-0.03}$	$0.017^{+0.002}_{-0.002}$	$1.4^{+0.4}_{-0.4}$	$1.020^{+0.002}_{-0.002}$	$1.020^{+0.003}_{-0.002}$	...	1016.9/1014
405057020	...	...	$1.343^{+0.001}_{-0.001}$	$0.05^{+0.01}_{-0.01}$	$2.4^{+0.1}_{-0.1}$	$0.1^{+0.3}_{-0.1}$	$1.077^{+0.002}_{-0.002}$	$1.081^{+0.003}_{-0.001}$	...	...
405057030	...	...	$1.310^{+0.001}_{-0.001}$	$0.05^{+0.01}_{-0.01}$	$4.5^{+0.1}_{-0.1}$	$1.3^{+0.4}_{-0.4}$	$1.066^{+0.003}_{-0.004}$	$1.056^{+0.004}_{-0.004}$	...	...

Notes. Errors are 90% confidence level for one interesting parameter, except for the 0.8–8 keV (absorbed) flux error which is from the standard deviation of the XIS detector cross-normalizations. N_H is the neutral column; N_{eqp} is the `eqpair` normalization (see the text); kT_{disk} is the peak temperature of the disk seed photons; ℓ_h/ℓ_s is the relative corona to disk compactness (ℓ_s is fixed to 1); τ_{net} is the net coronal optical depth (including pair production); N_γ is the Gaussian line normalization in units of photons $cm^{-2}\,s^{-1}$; and C_{xisN} are the normalization constants for the XIS 0 and 3 detectors, relative to the XIS 1 detector. The first group of parameters are for data that include only statistical errors, while the second group of parameters are for data that also include 1.35% systematic errors.

Gaussian lines to the fits; however, as their presence is not strongly confirmed and there is no good evidence for a narrow line in either these spectra nor in the previously examined *Chandra*-HETG spectra (Nowak et al. 2008), we tie all the line energies (constrained to lie between 6.2 and 6.9 keV) and widths (fixed to 0.3 keV), and let only the line normalizations remain free.

The results of these fits are presented in Figure 5, and the parameters are given in Table 2. Overall, the quality of the fits is very good, yielding $\chi^2_\nu/\nu = 1756/1014 = 1.74$. Although the reduced χ^2 is not 1, the addition of only 1.35% systematic uncertainties to each data set brings the value down to that

level, without significantly altering the best-fit parameters, as also shown in Table 2. The addition of systematic uncertainties slightly increases the parameter error bars.

Given the obvious systematic differences between the frontside (XIS 0 and 3) and backside (XIS 1) detectors, seen in the residuals presented in Figure 5, we speculate that our fits are near "optimal". Throughout the rest of this work, the figures will include only statistical errors; however, tables will include sets of parameters with error bars that were calculated for spectra to which 1.35% systematic errors have been applied. This systematic error amplitude was chosen on the basis that it yields a reduced χ^2 value of ≈ 1 for the fits described above,
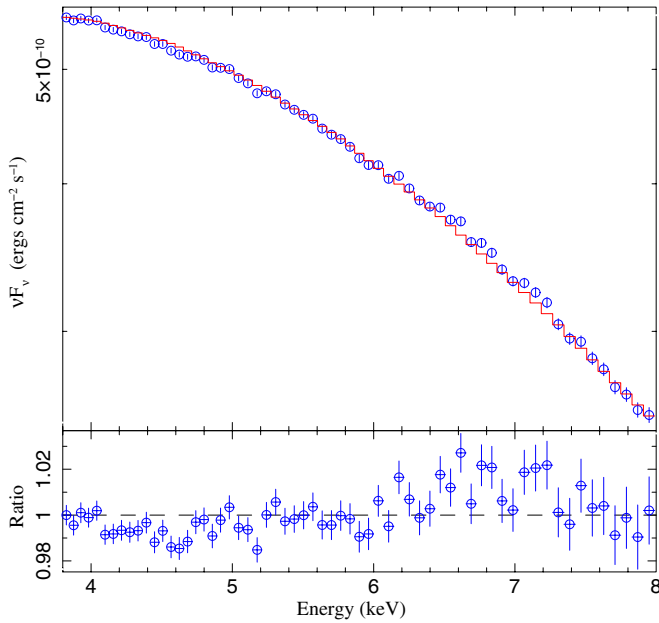
Figure 6. Simultaneous fit to all three observations using the `eqpair` model, but excluding the broad Gaussian line in the Fe region. (The spectra were combined for the plot, but not the fits.)

(A color version of this figure is available in the online journal.)

and we retain this level in subsequent model fits for ease of comparison.

The primary difference among the three spectra is the disk peak temperatures, which range between 1.31 and 1.48 keV. The coronal contribution is relatively weak, given the low values of the coronal compactness compared to the disk compactness, ℓ_h/ℓ_s. It is interesting to note that the two fainter observations indicate less energetic coronae—ℓ_h/ℓ_s values are lower—but higher optical depth ones. (Coronal compactness is its input energy divided by a characteristic radius, here measured relative to a compactness for the disk. If geometric changes are absent, then a lower fitted compactness is indicating a less energetic corona.) The resulting equilibrium coronal temperatures for the three observations are ≈600 keV, ≈2.2 keV, and ≈1.3 keV, respectively. When combined with their equilibrium optical depths, we find that the resulting Compton y-parameters range from 0.1 to 0.2. That is, Comptonization is only inducing a modest shift in the average photon energy. However, given the fact that we do not have a good spectrum above 8 keV, there is not a strong enough lever arm on these Comptonization fits to say how free from systematic uncertainty these parameter values are.

Likewise, detections of a (broad) Gaussian line peaking between 6.2 and 6.9 keV are marginal. The upper limits of the line strengths found here (in terms of integrated photon flux) are comparable to the estimated values from our prior *RXTE* observations, after taking into account the fact that *RXTE* also integrates line emission from the galactic ridge and likely had remaining systematic Fe line residuals at the $\approx1\%$ level (Nowak et al. 2008). That is, these line strengths are marginally consistent with the *RXTE* results. Furthermore, the line fitted here may be partly substituting for general spectral hardening at $\gtrsim6$ keV. It is clear, however, that any real line at the levels suggested by the *RXTE* observations cannot be narrow; any such line must be broad and have a peak residual relative to the continuum of $\lesssim2\%$. We illustrate this in Figure 6, wherein

we have refit the spectra excluding the Fe line, and combine all three observations in the plot—but not the fit—to show the Fe region residuals.

The most salient feature of these fits is that a model with a single normalization constant is both successful and yields a fairly small normalization of $\approx1.9\times10^{-4}$. The `eqpair` model normalization is proportional to the disk flux that would be observed in the absence of Comptonization, and is the same as the normalization of the `diskpn` model (Gierliński et al. 1999), namely

$$N_{\text{eqp}} = \left(\frac{M}{1\,M_\odot}\right)^2 \left(\frac{D}{1\,\text{kpc}}\right)^{-2} f_c^{-4}\cos i, \qquad (1)$$

where M is the central object mass, D is the distance, i is the disk inclination, and f_c is the color-correction factor of the disk (see also Coppi 1999). For a mass of $3\,M_\odot$, a distance of 10 kpc, and an inclination of $i = 75°$, we expect a normalization of $\approx3\times10^{-3}$, a factor of 15 times higher than observed. (The discrepancy only increases for a more face-on geometry; a more highly inclined geometry is unlikely given the lack of eclipses.) The fitted normalization can be recovered if we increase the distance to 40 kpc, increase the color-correction factor for the seed input photons to 3.3, or we decrease the characteristic emission radius by a factor of four. (The emitting area dependence is responsible for the M^2 term in the normalization.)

The `diskpn` model, which provides the seed photons for the `eqpair` model, has its peak emission radius at $\approx10\,GM/c^2$. If this radius were shrunk to $2.5\,GM/c^2$, the fitted normalization can be recovered with $M = 3\,M_\odot$, $D = 10$ kpc, and $i = 75°$. This is what we essentially now do by considering model fits with the `kerrbb` model. The `kerrbb` model (Li et al. 2005) uses a relativistic model of the disk structure, and includes Doppler beaming and gravitational redshift in calculation of the emergent spectrum. The spin of the black hole becomes a fit parameter. Increasing the spin from 0 (i.e., a Schwarzschild black hole) has two major effects: it increases the accretion efficiency of the disk and decreases the disk inner radius. These two effects in combination tend to increase the disk temperature while decreasing its normalization (i.e., emitting area or, equivalently, inner radius). Both of these effects are suggested in the 4U 1957+11 spectra.

Here, we adopt the exact same set of parameters that we considered for our prior studies of the *RXTE* spectra of 4U 1957+11 (Nowak et al. 2008). We assume a disk inclination of $i = 75°$, the theoretically preferred color-correction value of $f_c = 1.7$ (Davis et al. 2005, 2006) for the disk spectrum, and choose two sets of parameters: $3\,M_\odot$ and 10 kpc, and $16\,M_\odot$ and 22 kpc. We discuss these latter two choices more fully in Section 4. We further modify these fits by allowing for a spectral hardening which we model with `simpl` (Steiner et al. 2009), which is a convolution model that mimics some aspects of *optically thin* Comptonization.[9] The two parameters of this convolution model are the slope of the power law into which disk photons are transferred, and the fraction of input photons transferred into the hard tail.

---

[9] `simpl`, however, should not be confused with a Comptonization model. Aside from lacking any physical parameters, e.g., a coronal optical depth, a coronal temperature or compactness, and any reference to coronal geometry, it also cannot mimic spectral shapes associated with optically thick Comptonization. It should be regarded as purely a phenomenological model, albeit one that is more useful than a power law since it does not extend its spectrum to low energies in the same manner as a steep power law can.
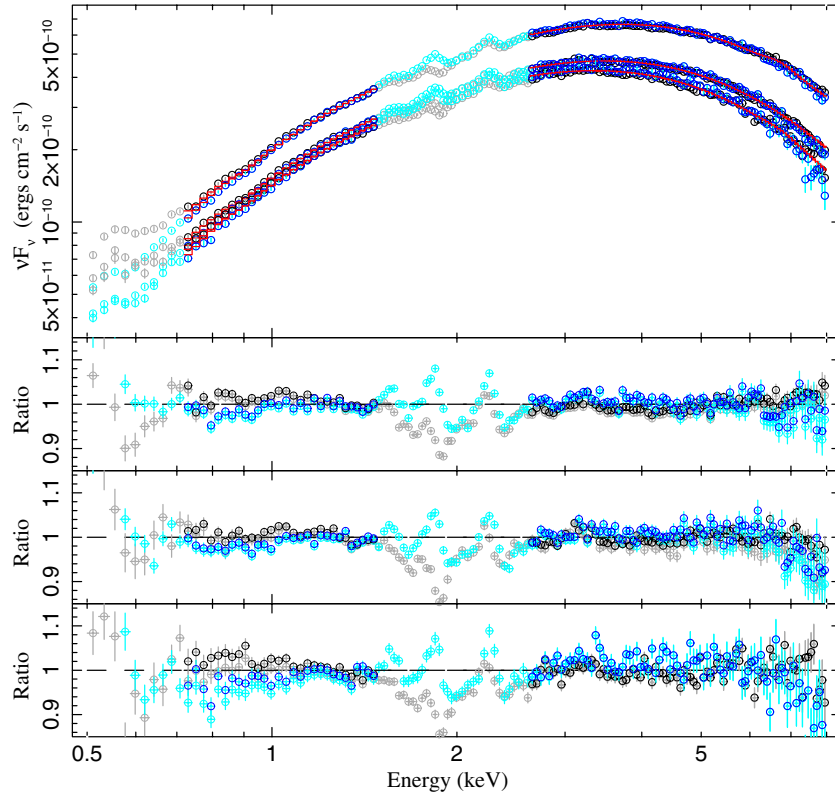
Figure 7. Joint fit of a `simpl⊗kerrbb` model to the three spectra assuming a black hole mass and distance of $16\,M_\odot$ and 22 kpc. The spectra share a common interstellar absorption column, black hole mass and spin, disk inclination, and a fixed color correction factor of $f_c = 1.7$. They have independent disk accretion rates and `simpl` parameters. Black/gray spectra are the combined XIS 0 and 3 spectra, and blue/light blue are the XIS 1 spectra. Lightly shaded data were not included in the fit. The top residuals' panel shows the ratio residuals for ObsID 405057010, the middle residuals' panel shows the ratio residuals for ObsID 405057020, and the bottom shows the ratio residuals for ObsID 405057030.

(A color version of this figure is available in the online journal.)

Table 3
`constant*TBnew*simpl⊗(kerrbb+gaussian)` Fits to 4U 1957+11 Spectra

ObsID	$N_{\rm H}$ $(10^{21}\,{\rm cm}^{-2})$	a^* (Jc/GM^2)	$\dot{M}$ $(10^{17}{\rm g\,s}^{-1})$	Γ	$f_{\rm scat}$	N_γ (10^{-4})	$C_{\rm xis0}$	$C_{\rm xis3}$	$\chi^2/{\rm dof}$
405057010	$0.185^{+0.002}_{-0.001}$	$0.8965^{+0.0011}_{-0.0012}$	$0.180^{+0.001}_{-0.001}$	$1.1^{+2.9}_{-0.0}$	$0.000^{+0.001}_{-0.000}$	$0.9^{+0.4}_{-0.4}$	$1.019^{+0.002}_{-0.002}$	$1.020^{+0.002}_{-0.002}$	2062.5/1014
405057020	$\cdots$	$\cdots$	$0.131^{+0.001}_{-0.001}$	$1.1^{+0.1}_{-0.0}$	$0.037^{+0.004}_{-0.004}$	$0.0^{+0.1}_{-0.0}$	$1.078^{+0.003}_{-0.003}$	$1.083^{+0.003}_{-0.003}$	$\cdots$
405057030	$\cdots$	$\cdots$	$0.115^{+0.002}_{-0.001}$	$4.0^{+0.0}_{-1.3}$	$0.015^{+0.006}_{-0.008}$	$0.0^{+0.2}_{-0.0}$	$1.067^{+0.005}_{-0.004}$	$1.057^{+0.004}_{-0.005}$	$\cdots$
405057010	$0.186^{+0.002}_{-0.001}$	$0.8957^{+0.0016}_{-0.0016}$	$0.181^{+0.001}_{-0.002}$	$1.1^{+2.9}_{-0.0}$	$0.000^{+0.002}_{-0.000}$	$1.0^{+0.5}_{-0.5}$	$1.021^{+0.003}_{-0.004}$	$1.021^{+0.003}_{-0.004}$	1189.8/1014
405057020	$\cdots$	$\cdots$	$0.131^{+0.001}_{-0.002}$	$1.1^{+0.1}_{-0.0}$	$0.032^{+0.005}_{-0.006}$	$0.0^{+0.1}_{-0.0}$	$1.077^{+0.004}_{-0.004}$	$1.081^{+0.004}_{-0.004}$	$\cdots$
405057030	$\cdots$	$\cdots$	$0.116^{+0.002}_{-0.002}$	$4.0^{+0.0}_{-2.5}$	$0.009^{+0.008}_{-0.005}$	$0.0^{+0.3}_{-0.0}$	$1.067^{+0.006}_{-0.006}$	$1.056^{+0.006}_{-0.006}$	$\cdots$
405057010	$0.171^{+0.002}_{-0.002}$	$0.9991^{+0.0002}_{-0.0001}$	$0.288^{+0.007}_{-0.005}$	$1.4^{+0.1}_{-0.1}$	$0.072^{+0.009}_{-0.007}$	$2.3^{+0.5}_{-0.5}$	$1.021^{+0.003}_{-0.002}$	$1.021^{+0.003}_{-0.002}$	1830.0/1014
405057020	$\cdots$	$\cdots$	$0.224^{+0.005}_{-0.004}$	$1.1^{+0.1}_{-0.0}$	$0.150^{+0.007}_{-0.007}$	$0.1^{+0.4}_{-0.1}$	$1.080^{+0.003}_{-0.003}$	$1.085^{+0.003}_{-0.003}$	$\cdots$
405057030	$\cdots$	$\cdots$	$0.176^{+0.003}_{-0.004}$	$3.4^{+0.6}_{-0.4}$	$0.127^{+0.032}_{-0.022}$	$0.7^{+0.6}_{-0.5}$	$1.069^{+0.005}_{-0.004}$	$1.058^{+0.004}_{-0.005}$	$\cdots$
405057010	$0.171^{+0.002}_{-0.002}$	$0.9993^{+0.0002}_{-0.0002}$	$0.282^{+0.007}_{-0.007}$	$1.4^{+0.2}_{-0.1}$	$0.068^{+0.010}_{-0.008}$	$2.1^{+0.6}_{-0.5}$	$1.022^{+0.004}_{-0.003}$	$1.022^{+0.003}_{-0.004}$	1084.3/1014
405057020	$\cdots$	$\cdots$	$0.219^{+0.007}_{-0.006}$	$1.1^{+0.1}_{-0.0}$	$0.142^{+0.009}_{-0.010}$	$0.2^{+0.5}_{-0.2}$	$1.080^{+0.004}_{-0.003}$	$1.083^{+0.004}_{-0.004}$	$\cdots$
405057030	$\cdots$	$\cdots$	$0.173^{+0.004}_{-0.004}$	$3.7^{+0.7}_{-0.3}$	$0.128^{+0.026}_{-0.030}$	$0.9^{+0.6}_{-0.6}$	$1.068^{+0.007}_{-0.005}$	$1.057^{+0.006}_{-0.006}$	$\cdots$

Notes. Errors are 90% confidence level for one interesting parameter. $N_{\rm H}$ is the neutral column; a^* is the black hole dimensionless spin; $\dot{M}$ is the disk accretion rate; f_c, the disk color-correction factor, has been fixed to 1.7; Γ and $f_{\rm scat}$ are the `simpl` parameters (power-law slope, constrained to lie between 1.1 and 4, and fraction of scattered continuum); N_γ is the Gaussian line normalization in units of photons cm^{-2} s^{-1}; and $C_{\rm xisN}$ are the normalization constants for the XIS 0 and 3 detectors, relative to the XIS 1 detector. The top set of parameters are for a black hole mass of $3\,M_\odot$ and a distance of 10 kpc, while the bottom set are for a mass and distance of $16\,M_\odot$ and 22 kpc. Within each set of parameters, the first group are for data that include only statistical errors, while the second group are for data that also include 1.35% systematic errors.

As for the Comptonization models, we fit all three observations simultaneously, include a broad Gaussian line in exactly the same manner, and tie some of the model parameters together. Specifically, we constrain each observation to be fit with the same neutral column, line energy and width (fixed to 0.3 keV), and black hole spin, but let the disk accretion rate, the `simpl` model parameters, and the line normalization be free. Results for these `kerrbb` model fits are presented in Table 3 and Figure 7.

The resulting fits are good, with the 3 $M_\odot$, 10 kpc model yielding $\chi_\nu^2/\nu = 2063/1014$ and the 16 $M_\odot$, 22 kpc model yielding $\chi_\nu^2/\nu = 1830/1014$. The latter model is very comparable to our best Comptonization fit. Additionally, this latter, more successful, model has line parameters very similar to those from the Comptonization fits. We also find that only $\approx 7\%$–15% of the disk photons are transferred into a hard tail. The fitted neutral column is slightly smaller than for the Comptonization fits, but only by $\lesssim 10\%$.

Just as the Comptonization models could fit all three observations with a constant normalization (equivalent to a constant inner disk radius), so too can the relativistic disk models fit all three observations with a constant spin parameter (also equivalent to a constant inner disk radius). The main variable parameter among the observations here becomes the disk accretion rate. For both sets of mass and distance assumptions, the fitted spin parameter is high: nearly 0.9 for the 3 $M_\odot$, 10 kpc case, and nearly maximally spinning in the other. We discuss the scaling relations among the disk parameters in the next section.

4. SCALING RELATIONS

As shown above, spectral fits to the data are somewhat degenerate. We have found a successful set of relativistic disk model fits assuming a mass of 3 $M_\odot$ and a distance of 10 kpc, and also when assuming a mass of 16 $M_\odot$ and a distance of 22 kpc. The first set of parameters was chosen as being the lowest mass/closest distance black hole that is likely to be consistent with 4U 1957+11 persistently remaining in a soft state. The second set of parameters was chosen to be consistent with our prior *RXTE* studies (Nowak et al. 2008), which in turn were found via the scaling relations described below.

As the spectra are dominated by the seed photons from a disk for both the disk and Comptonization models, the flux, F, scales as

$$F \propto \frac{R^2}{D^2} T_{\rm eff}^4 \propto \frac{M^2}{D^2} \left(\frac{T_{\rm col}}{f_c}\right)^4, \qquad (2)$$

where D is the distance to the source, R is the inner radius of the disk, M is the black hole mass, $T_{\rm eff}$ is the disk's peak effective temperature, $T_{\rm col}$ is the disk's peak color temperature, and f_c is the color correction factor. The effective temperature to the fourth power scales as the fractional Eddington luminosity, $L/L_{\rm Edd}$, multiplied by $M/R^2 \propto M^{-1}$. Thus, if we make the assumption that the lowest flux *RXTE* observations described by Nowak et al. (2008) are indeed at a fixed fraction of Eddington luminosity, e.g., 3%, then we will have

$$\left(\frac{T_{\rm col}}{f_c}\right)^4 \propto M^{-1}. \qquad (3)$$

The color temperature is fixed by observation, and $L/L_{\rm Edd} \propto \dot{M}/M$ (where $\dot{M}$ is the accretion rate) is fixed by assumption, leading to the first two of our scaling relations:

$$M \propto f_c^4, \qquad \dot{M} \propto f_c^4. \qquad (4)$$

Just as the color temperature is fixed by observations, so too is the flux. Given that the disk inner radius scales as mass, and using the fact that the color temperature and flux are fixed by observation, we have that $M^2/D^2 f_c^4$ is fixed. Using the above scaling relations, we then obtain
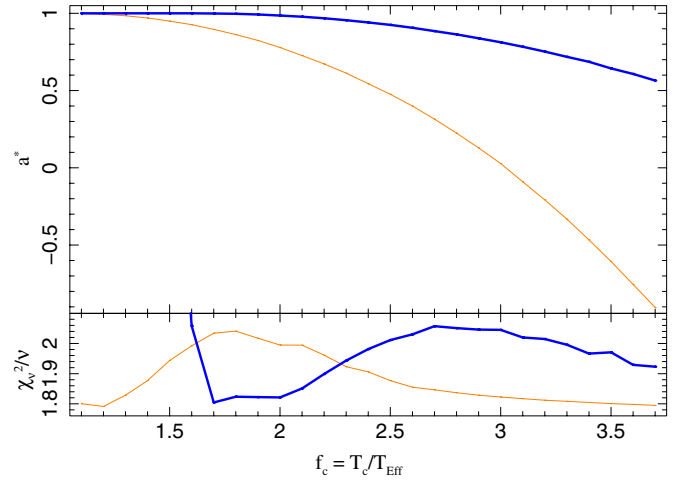
$$D \propto f_c^2. \qquad (5)$$

Figure 8. Results of fitting a `simpl⊗kerrbb` to the three *Suzaku* observations of 4U 1957+11. The top panel shows the fitted spin vs. spectral hardening factor. The bottom panel shows the reduced χ^2 value of the fits. The blue (thicker) lines represent models with the mass and distance fixed to 16 $M_\odot$ and 22 kpc, respectively, and orange lines represent models with the mass and distance fixed to 3 $M_\odot$ and 10 kpc, respectively.

(A color version of this figure is available in the online journal.)

We have previously used these scaling relations to find spectral fits for a black hole mass of 16 $M_\odot$ and a distance of $\approx$22 kpc (Nowak et al. 2008). Specifically, we first explored fits to *RXTE* spectra where we fixed the mass and distance to 3 $M_\odot$ and 10 kpc. We found that the best fits clustered around a spectral hardening factor of $f_c \approx 1.1$. We then fixed the spectral hardening factor to $f_c = 1.7$ and the mass to 16 $M_\odot$. We allowed the distance to be a free parameter, and found that its best-fit values clustered around 22 kpc, i.e., roughly consistent with the scaling relations above.

Here we perform a similar exercise for the *Suzaku* spectra. As in Section 3, we fit all three spectra simultaneously with the `simpl⊗kerrbb` model wherein we only allow the accretion rate and `simpl` parameters to vary among the three spectra. We consider two sets of fits, one with mass of 3 $M_\odot$ and distance 10 kpc, and another with 16 $M_\odot$ and distance 22 kpc. For both we allow the black hole spin to be a free parameter, and we create grids of fits for fixed spectral hardening factors ranging over $f_c = 1.1$–3.7. The plot of fitted spin, a^*, versus spectral hardening factor, f_c, is presented in Figure 8.

As for our prior *RXTE* observations, we find that fits using 3 $M_\odot$, 10 kpc, and $f_c = 1.1$ or 16 $M_\odot$, 22 kpc, and $f_c = 1.7$ are nearly equally good and are of comparable χ^2 to our best Comptonization fits. We also see that all fits using 16 $M_\odot$ and 22 kpc require large spin parameters. The fits using 3 $M_\odot$ and 10 kpc only achieve low spin parameters for large color correction factors, $f_c \gtrsim 3$. (These conclusions are unaltered if uniform 1.35% systematic errors are included in the fits.)

5. DISCUSSION

There are four salient features of these *Suzaku* observations of 4U 1957+11 that echo the results that we obtained with our prior *Chandra*, *XMM-Newton*, and *RXTE* studies. The peak disk temperatures are high, the disk normalizations (or equivalently, emitting areas or inner disk radii) are small, all observations can be fit with the same inner disk radius, and the spectra are remarkably simple. The only significant deviations from a simple continuum, aside from spectral hardening and a possible
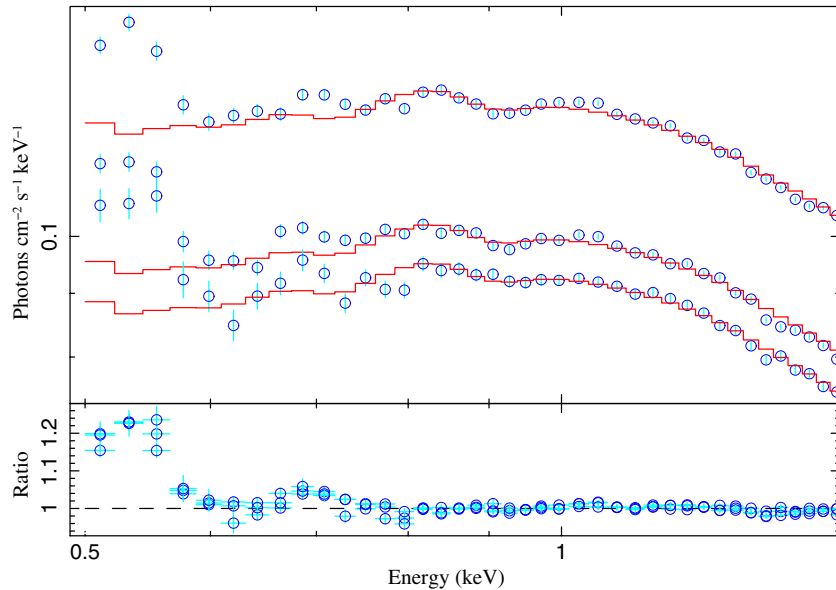
Figure 9. Same fit as seen in Figure 5, but showing the XIS 0, 1, and 3 spectra combined, and the model applied down to 0.5 keV.
(A color version of this figure is available in the online journal.)

weak, broad Fe line at high energy, are ≈ 0.7–0.9 keV features associated with absorption by the ISM, predominantly due to the Fe L and Ne edges.

We show a closeup of this region in Figure 9. The spectral feature seen at ≈ 0.55 keV, not described by our fitted models, can in fact be seen in the flux corrected spectra of *any* monochromatic, narrow line spectrum simulated using the *Suzaku* response functions. Small calibration errors in the amplitude of this feature potentially could lead to a systematic underestimate or overestimate of the predicted counts near 0.55 keV. We thus do not believe that this feature is indicative of physical complexity in the underlying 4U 1957+11 spectra. Likewise, it is unclear whether the $\approx 5\%$ residuals seen near the 0.7 keV Fe L edge represent complexity in the physical spectrum, as opposed to uncertainty in the response. Aside from the Fe L edges, *Chandra* and *XMM-Newton* spectra did not show any spectral features near the 0.7 keV bandpass (Nowak et al. 2008).

The only clear spectral features are the Ne edge/Ne IX absorption near 0.9 keV. Similarly simple disk spectra were implied by *Suzaku* observations of LMC X-3 in its soft, disk-dominated state (Kubota et al. 2010). As pointed out by Kubota et al. (2010), such spectral simplicity is in fact surprising if modern disk atmosphere models apply to these sources. These disk atmosphere models predict spectral structure with $\pm 5\%$ amplitude near metal edges (Davis & Hubeny 2006) that is seen neither here nor in *Suzaku* observations of LMC X-3. That the simplest, phenomenological disk models lacking such features describe the spectra extremely well (i.e., to within $\lesssim 5\%$ 0.7–0.8 keV, and to $\lesssim 2\%$ above 0.8 keV) is quite remarkable and may indicate that additional physics needs to be incorporated into the disk atmosphere models (Kubota et al. 2010).

We also have confirmed the results of our prior studies in that the best fits assuming a small mass and distance (3 $M_\odot$, 10 kpc) require a black hole spin $a^* \gtrsim 0.9$. The required spin increases if we instead assume 16 $M_\odot$ and 22 kpc. Altering the assumed disk inclination does not change this situation. Higher disk inclinations are ruled out by the lack of system eclipses.

Lower disk inclinations allow for more observed gravitational redshifting, and less relativistic beaming, of the spectrum, and thus require larger spectral correction factors (i.e., inclination effects more than just the projected area of the disk.) As an example, we took the 16 $M_\odot$ and 22 kpc `kerrbb` model, froze the inclination to 45°, and let both the black hole spin and hardness correction factor become free parameters. A solution with χ^2 comparable to the best fits discussed above was found, however, it required *maximally negative spin* of $a^* \approx -1$ and an extremely large color correction factor of ≈ 8. Thus, high-spin/high-inclination solutions are the most "straightforward" solutions that we have been able to obtain, and generally have had the lowest color-correction factors of the models that we have explored (see also Nowak et al. 2008).

These results are in fact confirmed by the Comptonization model fits: the high disk temperatures (1.31–1.48 keV) and especially the low normalization—15 times lower than expected for a 3 $M_\odot$ Schwarzschild black hole at 10 kpc—could be indicative of a rapidly spinning black hole. As discussed above, the disk temperature in the `diskpn` seed photons used in the Comptonization model peaks at $\approx 10\,GM/c^2$. If one were to reduce this radius to $\approx 2.5\,GM/c^2$, i.e., change the emission profile to more closely match that of a rapidly spinning hole, then the Comptonization model normalization would be consistent with a 3 $M_\odot$ black hole at only 10 kpc.

The Comptonization models offer two possibilities[10] for fitting the 4U 1957+11 spectrum with a low spin. The first, perhaps less likely, possibility is to increase the color-correction factor via a low-temperature, optically thick corona. We have already seen that the lowest flux observations are fit with such coronae, albeit with a Compton y-parameter of ≈ 0.1. Instead, we are envisioning a scenario wherein $y \approx f_c \approx 3$—the color-correction value required to fit a 3 $M_\odot$, 10 kpc, Schwarzschild

---

[10] Note that we are ignoring issues of the unknown inclination. Choosing a more face-on inclination only exacerbates the normalization problem (i.e., we would have expected an even larger normalization), and would introduce more gravitational redshifting to the observed temperature, increasing the requirement for rapid spin in the spectral fits.

black hole. This would require an optical depth of

$$\tau \approx 9.8 \left(\frac{4\,\mathrm{keV}}{kT_\mathrm{c}}\right)^{1/2} \left(\frac{f_\mathrm{c}}{3}\right)^{1/2}, \qquad (6)$$

where kT_c is the coronal temperature. This is a coronal regime typically not explored in spectral models. The concept would be that the low-flux, equilibrium solution of the disk was such a cool, optically thick atmosphere which at higher flux (i.e., the 15% of the time requiring a hard tail) expanded into a hot, optically thin corona.

Aside from lacking a theoretical description of such a scenario, the fitted constant emitting area at low flux implies that the 4U 1957+11 system must always return to the *same* equilibrium coronal solution at low flux. It is not clear why this should be the case. The second possibility offered by the Comptonization solutions is simply to increase the distance to 4U 1957+11, while keeping the mass small. The scaling relations discussed in Section 4 only apply under the assumption that the lowest flux observations are a fixed fraction of the Eddington luminosity (e.g., 2% L_Edd). If we relax this assumption, then Equation (1) suggests that if the 4U 1957+11 distance were 40 kpc, then it could be a 3 $M_\odot$ Schwarzschild black hole. This would imply, however, that the *faintest* 4U 1957+11 spectra are $\gtrsim$30% L_Edd, while the brightest observed *RXTE* spectra are $\gtrsim L_\mathrm{Edd}$. This would be rather unusual, especially given the lack of strong variability found in the *RXTE* spectra: the root-mean-square variability is typically $\lesssim$3%, and at its strongest was $\lesssim$13% in the 2–60 keV bandpass over $\approx$$10^{-2}$ to 2×10^3 Hz (Nowak & Wilms 1999; Nowak et al. 2008).

It therefore seems likely that 4U 1957+11 is a system that has a combination of both high spin and large distance, which puts this X-ray binary in the Galaxy's halo. It is interesting to speculate whether these two characteristics are related to one another. First, we note the obvious fact that in order for 4U 1957+11 to be an X-ray binary it must still be accreting and therefore be a comparatively young system. Given the low star formation rate in the Galaxy's halo, it is rather unlikely, therefore, that 4U 1957+11 was formed in the halo. Instead 4U 1957+11 likely originates in the Galactic disk and then migrated into the halo. Several possible formation scenarios have been discussed in the literature, most recently associated with the discovery of young hypervelocity stars in the Galaxy's halo. For example, Perets (2009, and references therein) discuss a scenario where hypervelocity binary systems are created through the interaction of a hierarchical triple star system with the supermassive black hole in the center of the Galaxy. Since hierarchical triples are very common among multiple star systems, such a scenario is likely. With a typical ejection velocity of 1800 km s^{-1}, it would take this system a few 10^6 years to reach its current position, well within the lifetime of typical evolution scenarios for X-ray binary systems (van den Heuvel 1976). (At such a velocity, and assuming a 22 kpc distance, the proper motion of 4U 1957+11 likely would have amounted to $\lesssim$0″.3 since the discovery of the optical counterpart by Margon et al. 1978.) Such a scenario

could also explain a large spin for the system, if during the ejection angular momentum is transferred onto the black hole.

A high black hole spin for 4U 1957+11 is a consistent interpretation of the results presented here; however, such a result is dependent upon the unknown mass, distance, and inclination of the system. Given the nature of 4U 1957+11 as perhaps the simplest, cleanest example of a BHC soft state, and perhaps the most rapidly spinning black hole, observations to independently determine this system's parameters are urgently needed.

REFERENCES

Bayless, A., Robinson, E., Mason, P., & Robertson, P. 2011, ApJ, 730, 43
Coppi, P. 1999, PASP, 161, 375
Davis, S. W., Blaes, O. M., Hubeny, I., & Turner, N. J. 2005, ApJ, 621, 372
Davis, S. W., Done, C., & Blaes, O. M. 2006, ApJ, 647, 525
Davis, S. W., & Hubeny, I. 2006, ApJS, 164, 530
Dunn, R. J. H., Fender, R. P., Körding, E. G., et al. 2010, MNRAS, 403, 61
Gierliński, M., Zdziarski, A. A., Poutanen, J., et al. 1999, MNRAS, 309, 496
Hakala, P. J., Muhli, P., & Dubus, G. 1999, MNRAS, 306, 701
Houck, J. C., & Denicola, L. A. 2000, in ASP Conf. Ser. 216, Astronomical Data Analysis Software and Systems IX, Vol. 9, ed. N. Manset, C. Veillet, & D. Crabtree (San Francisco, CA: ASP), 591
Koyama, K., Tsunemi, H., Dotani, T., et al. 2007, PASJ, 59, 23
Kubota, A., Done, C., Davis, S. W., et al. 2010, ApJ, 714, 860
Li, L.-X., Zimmerman, E. R., Narayan, R., & McClintock, J. E. 2005, ApJS, 157, 335
Maccarone, T. J. 2003, A&A, 409, 697
Margon, B., Thornstensen, J. R., & Bowyer, S. 1978, ApJ, 221, 907
Mitsuda, K., Bautz, M., Inoue, H., et al. 2007, PASJ, 59, 1
Mitsuda, K., Inoue, H., Koyama, K., et al. 1984, PASJ, 36, 741
Nowak, M. A., Hanke, M., Trowbridge, S. N., et al. 2011, ApJ, 728, 13
Nowak, M. A., Juett, A., Homan, J., et al. 2008, ApJ, 689, 1199
Nowak, M. A., & Wilms, J. 1999, ApJ, 522, 476
Nowak, M. A., Wilms, J., Heindl, W. A., et al. 2001, MNRAS, 320, 316
Perets, H. B. 2009, ApJ, 698, 1330
Russell, D. M., Lewis, F., Roche, P., et al. 2010, MNRAS, 402, 2671
Russell, D. M., Miller-Jones, J. C. A., Maccarone, T. J., et al. 2011, ApJ, 739, L19
Shafee, R., McClintock, J. E., Narayan, R., et al. 2006, ApJ, 636, L113
Shakura, N. I., & Sunyaev, R. 1973, A&A, 24, 337
Steiner, J. F., Narayan, R., McClintock, J. E., & Ebisawa, K. 2009, PASP, 121, 1279
Takahashi, T., Abe, K., Endo, M., et al. 2007, PASJ, 59, 35
Thorstensen, J. R. 1987, ApJ, 312, 739
Uchiyama, Y., Maeda, Y., Ebara, M., et al. 2008, PASJ, 60, 35
van den Heuvel, E. P. J. 1976, in IAU Symp. 73, Structure and Evolution of Close Binary Systems, ed. P. Eggleton, S. Mitton, & J. Whelan (Cambridge: Cambridge Univ. Press), 35
Wijnands, R., Miller, J., & van der Klis, M. 2002, MNRAS, 331, 60
Wilms, J., Allen, A., & McCray, R. 2000, ApJ, 542, 914
Wilms, J., Nowak, M. A., Pottschmidt, K., et al. 2001, MNRAS, 320, 316
Yao, Y., Nowak, M. A., Wang, Q. D., Schulz, N. S., & Canizares, C. R. 2008, ApJ, 672, L21